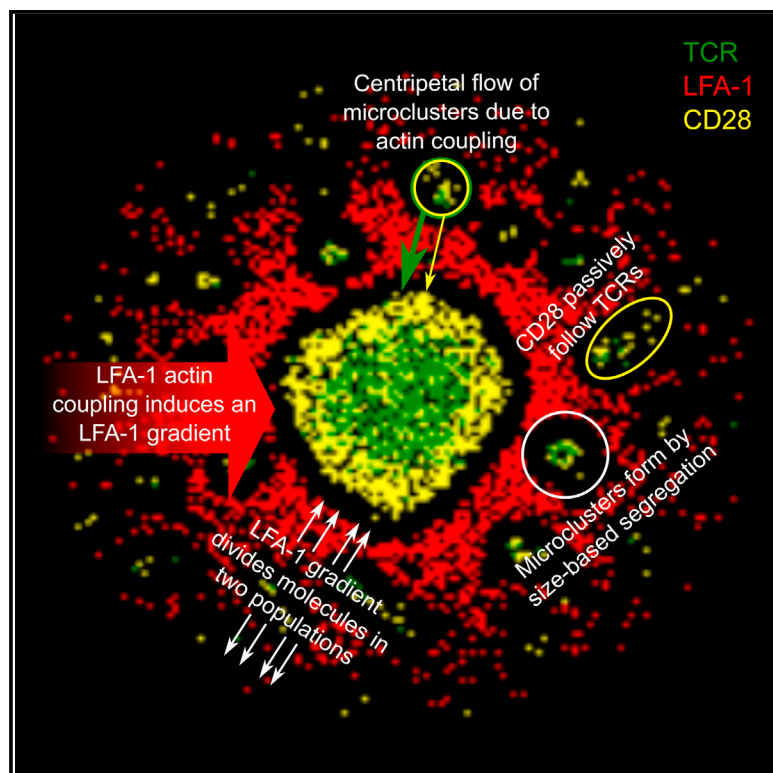


# F-Actin-Driven CD28-CD80 Localization in the Immune Synapse

## Graphical Abstract



## Authors

Anastasios Siokis, Philippe A. Robert, Philippos Demetriou, Michael L. Dustin, Michael Meyer-Hermann

## Correspondence

philippe.robert@ens-lyon.org (P.A.R.), mmh@theoretical-biology.de (M.M.-H.)

## In Brief

Siokis et al. analyze the impact of actin-derived forces on the positioning of molecules during immunological synapse formation. While CD28 can reach the center of the synapse by passively following TCR microclusters, the characteristic ring-like pattern of CD28 complexes requires coupling to actin.

## Highlights

- LFA-1 actin coupling generates an LFA-1 gradient
- LFA-1 gradient impacts the localization of other molecules in the synapse
- CD28 can passively follow TCR microclusters
- CD28 coupling to actin is necessary to obtain a proper CD28 localization



# F-Actin-Driven CD28-CD80 Localization in the Immune Synapse

Anastasios Siokis,<sup>1</sup> Philippe A. Robert,<sup>1,\*</sup> Philippos Demetriou,<sup>3</sup> Michael L. Dustin,<sup>3,4</sup> and Michael Meyer-Hermann<sup>1,2,5,\*</sup>

<sup>1</sup>Department of Systems Immunology and Braunschweig Integrated Centre of Systems Biology, Helmholtz Centre for Infection Research, Braunschweig 38106, Germany

<sup>2</sup>Institute of Biochemistry, Biotechnology and Bioinformatics, Technische Universität Braunschweig, Braunschweig 38106, Germany

<sup>3</sup>Kennedy Institute, Nuffield Department of Orthopedics, Rheumatology and Musculoskeletal Sciences, University of Oxford, Headington, Oxford OX3 7FY, UK

<sup>4</sup>Skirball Institute of Biomolecular Medicine, New York University School of Medicine, New York, NY 10016, USA

<sup>5</sup>Lead Contact

\*Correspondence: [philippe.robert@ens-lyon.org](mailto:philippe.robert@ens-lyon.org) (P.A.R.), [mmh@theoretical-biology.de](mailto:mmh@theoretical-biology.de) (M.M.-H.)

<https://doi.org/10.1016/j.celrep.2018.06.114>

## SUMMARY

During immunological synapse (IS) formation, T cell receptor (TCR) signaling complexes, integrins, and costimulatory molecules exhibit a particular spatial localization. Here, we develop an agent-based model for the IS formation based on TCR peptide-bound major histocompatibility complex (pMHC) and leukocyte-function-associated antigen 1 (LFA-1) intracellular activation molecule 1 (ICAM-1) dynamics, including CD28 binding to a costimulatory ligand, coupling of molecules to the centripetal actin flow, and size-based segregation (SBS). A radial gradient of LFA-1 in the peripheral supramolecular activation cluster (pSMAC) toward the central supramolecular activation cluster (cSMAC) emerged as a combined consequence of actin binding and diffusion and modified the positioning of other molecules. The simulations predict a mechanism of CD28 movement, according to which CD28-CD80 complexes passively follow TCR-pMHC microclusters. However, the characteristic CD28-CD80 localization in a ring pattern around the cSMAC only emerges with a particular CD28-actin coupling strength that induces a centripetal motion. These results have implications for the understanding of T cell activation and fate decisions.

## INTRODUCTION

The formation of immune synapses (ISs) is a central process for antigen recognition by T cells. The structure of the IS impacts on T cell activation, signaling, and fate decisions (Mossman et al., 2005; Alarcón et al., 2011; Manz et al., 2011; Lee et al., 2002, 2003; Sage et al., 2012; Tabdanov et al., 2015; Ortega-Carrion and Vicente-Manzanares, 2016), and a lot of attention has been placed toward understanding the mechanisms of IS formation (Grakoui et al., 1999; Dustin, 2014; Dustin and Depoil, 2011; Springer, 1990). During early IS forma-

tion, specific T cell receptors (TCRs) bind to peptide-bound major histocompatibility complexes (pMHC) and form islands of microclusters. Synapse formation and adhesion is stabilized by integrin complexes, formed between leukocyte-function-associated antigen 1 (LFA-1) and intracellular activation molecule 1 (ICAM-1). TCR-pMHC microclusters move to the central region of the contact interface, while LFA-1-ICAM-1 complexes encircle these microclusters. Later, the two kinds of complexes segregate from each other and form two distinct areas in the synapse: the central supramolecular activation cluster (cSMAC) occupied by TCR-pMHC complexes and the peripheral SMAC (pSMAC) formed by integrin complexes (Grakoui et al., 1999).

TCR signaling can be modulated by a variety of costimulatory molecules, among which CD28 carries a significant role for regulatory and follicular helper T cell differentiation (Wang et al., 2015; Sansom and Walker, 2006). Binding of CD28 to one of its major ligands, CD80 (B7-1) or CD86 (B7-2), supports TCR signaling (Acuto and Michel, 2003; Beyersdorf et al., 2015), while a lack of CD28 costimulation leads to an apathetic state known as anergy (Slavik et al., 1999; Acuto and Michel, 2003; Pentcheva-Hoang et al., 2004).

CD28 has been shown to be preferentially located in the cSMAC (Bromley et al., 2001). This particular localization was attributed to the ligation with CD86 (Pentcheva-Hoang et al., 2004) or CD80 (Tseng et al., 2005). A ring of CD28 around the cSMAC has been described (Tseng et al., 2005) and was further confirmed by the colocalization of CD28 and protein kinase C $\theta$  (PKC $\theta$ ) that also formed a ring around the cSMAC (Yokosuka et al., 2008; Sanchez-Lockhart et al., 2008; Tseng et al., 2008). The reasons for this characteristic pattern are still poorly understood. Full-length CD80 was shown to segregate CD28 from TCR complexes, whereas removal of its cytoplasmic domain allows colocalization with the TCR (Tseng et al., 2005). CD80 is not sufficient for proper CD28 localization, since a mutation in the cytosolic tail of CD28 leads to a disruption of the ring-like pattern (Sanchez-Lockhart et al., 2008). There is also evidence that CD28 binds to F-actin, since it has been shown to recruit filamin-A (FLNa), an actin-binding protein, upon ligation (Tavano et al., 2006; Hayashi and Altman, 2006). The hypothesis of cytoskeletal-driven motion is further supported by the observation of a linear motion of CD28 complexes toward the cSMAC (Pielak



et al., 2017), raising the question whether actin-driven forces could explain the localization of CD28.

Coupling of molecules to the inward flow of F-actin is believed to be the mechanism that drives microcluster movement. DeMond et al. (2008) introduced mazes of barriers on the supported lipid bilayer (SLB) surface and showed that TCR-pMHC movement is based on frictional coupling to F-actin centripetal flow. TCR-pMHC microclusters in Jurkat T cells are transported in the IS due the retrograde flow of F-actin and the contraction of actomyosin-II arcs (Yi et al., 2012; Basu and Huse, 2017). TCR microclusters and actomyosin arcs were found to travel together at a similar speed (Murugesan et al., 2016). F-actin flow in the IS drives the spatial organization and opening of LFA-1 in regions close to the cSMAC, a process called affinity maturation of LFA-1 (Comrie et al., 2015; Murugesan et al., 2016; Basu and Huse, 2017). Furthermore, F-actin polymerization and retrograde flow have been shown to be critical for microcluster movement (Beemiller et al., 2012; Yu et al., 2013) and PLC $\gamma$ 1 signaling (Babich et al., 2012). A centrally directed transport is likely not restricted to TCR-pMHC complexes, and it is not clear whether other molecules in the IS are also coupled to F-actin.

Different modeling approaches have been developed to understand the IS spatial formation based on mechanical forces, with the majority focusing on the microcluster formation mechanisms. Partial differential equation (PDE) models have shown that membrane bending can account for microcluster formation (Qi et al., 2001; Hori et al., 2002; Burroughs and Wülfing, 2002). Accordingly, elasto-hydrodynamics of the membrane and fluid flow in the synaptic cleft could explain how microclusters form (Carlson and Mahadevan, 2015). All of these models reproduced the formation of the cSMAC (in accordance with Grakoui et al., 1999) and explained microcluster formation with size-based segregation (SBS) (Springer, 1990), but SBS was not sufficient to confer the formation of a bull's eye pattern and TCR-pMHC accumulation in the cSMAC.

Based on findings from an experimental setting introduced by Mossman et al. (2005), agent-based models were used to design experiments with barriers on SLBs to discriminate whether a central force or a long range attraction of TCR-pMHCs drives the bull's eye pattern (Figge and Meyer-Hermann, 2006). The corresponding experimental results suggested a coordinated centripetal transport of TCRs linked to the centripetal cortical actin flow (DeMond et al., 2008). A Monte-Carlo approach with biased centrally directed diffusion of the complexes has also been considered (Tsourkas et al., 2007; Tsourkas and Raychaudhuri, 2010). A statistical mechanics study describing the collective behavior and the most probable distribution of a large number of particles based on their interactions suggested that cytoskeletal transport processes can successfully explain cSMAC formation (Weikl et al., 2002). These models were limited to microcluster formation and central forces on the TCRs and did not investigate the effect of actin on other functional molecules.

In this study, we developed an agent-based model based on SBS and centripetal F-actin transport of molecules with the aim to determine the mechanisms driving the particular localization of CD28-CD80. The model predicts that a combination of diffusion and attachment of LFA-1-ICAM-1 to the underlying F-actin network (Comrie et al., 2015; Murugesan et al., 2016) in-

duces a radial gradient of LFA-1-ICAM-1 in the pSMAC with the highest density near the cSMAC. Further, CD28-CD80 can reach the cSMAC as passive followers of the TCR-pMHC microcluster move toward the center of the IS. However, this process alone was insufficient to generate the experimentally observed ring of CD28 around the cSMAC. We show that CD28-actin coupling is necessary to reproduce this pattern *in silico* and that the strength of this coupling tightly regulates the amount of CD28-CD80 that reaches the ring.

## RESULTS

### Initial Model for IS Formation

In order to understand the mechanisms driving spatial organization of molecules in the IS, we start from an agent-based model taking into account TCR, LFA-1, pMHC, and ICAM-1 only (see [Experimental Procedures](#)). Molecules are located in two lattices representing the membranes of two interacting cells. Free molecules may bind to their cognate ligand on the opposite lattice and already formed complexes can return to the free-molecule state according to their respective dissociation constants ([Table 1](#); [Figge and Meyer-Hermann, 2009](#)). Molecules and complexes move according to diffusion, SBS, or actin-mediated forces ([Figure 1](#)). SBS is modeled as a repulsive force between two complexes of different length ([Springer, 1990](#)). SBS alone generated TCR microclusters, but they failed to merge into the central SMAC ([Figure S1A](#)) and did not create the experimentally observed bull's eye pattern. This suggests that additional forces are needed for its formation.

A phenomenological representation of a centrally directed force was introduced to the model, which represents actin coupling of molecules inducing a centripetal flow. The strength of the force reflects the coupling strength to F-actin arcs. It was initially applied only to TCR-pMHC complexes ([Figure 2Aa–2Ac](#)). Microclusters formed since the first minute of contact between the cells, merged into bigger clusters, and finally formed the cSMAC ([Figure 2Ac](#); [Video S1](#)). The mature synapse formed at 10 min and remained stable, in agreement with experimental results ([Varma et al., 2006](#)). This *in silico* framework recapitulates the major properties of the IS and is suitable to investigate the properties of additional mechanisms and regulatory molecules.

### LFA-1's Interaction with the Actin Network Generates a pSMAC Gradient toward the Center

It has been suggested that LFA-1-ICAM-1 complexes can also be affected by the centripetal flow of F-actin arcs. A centripetal force on LFA-1 was added to the *in silico* model, and the predicted impact on IS formation was analyzed ([Figures 2Ad–2Af](#); [Video S2](#)). The localization of TCR-pMHC microclusters and the bull's eye were mainly unaffected, although the microclusters moved slower to the cSMAC due to higher density of LFA-1 around the cSMAC ([Video S1](#)). The density of complexes was computed inside equally spaced rings as the fraction of grid points occupied by each type of complex ([Figure 2B](#)). The model predicts the formation of an LFA-1 density gradient in the pSMAC. Without attachment to F-actin, LFA-1-ICAM-1 complexes were uniformly spread throughout the pSMAC (red solid

**Table 1. Parameter Values of the Reference**

| Name                                             | Parameter (Units)                        | Value           |
|--------------------------------------------------|------------------------------------------|-----------------|
| Radius of contact region                         | $R$ ( $\mu\text{m}$ )                    | 4.9             |
| Lattice constant                                 | $\alpha$ ( $\mu\text{m}$ )               | 0.07            |
| Free-molecule diffusion constant                 | $D_m$ ( $\mu\text{m}^2/\text{s}$ )       | 0.10            |
| Complex diffusion constant                       | $D_c$ ( $\mu\text{m}^2/\text{s}$ )       | 0.06            |
| Radius of SBS between TCR-pMHC and LFA-1-ICAM-1  | $R_{\text{SBS,TM-LI}}$ ( $\mu\text{m}$ ) | 0.425           |
| Weight of SBS between TCR-pMHC and LFA-1-ICAM-1  | $W_{\text{SBS,TM-LI}}$                   | −1.0            |
| Radius of SBS between CD28-CD80 and LFA-1-ICAM-1 | $R_{\text{SBS,CC-LI}}$ ( $\mu\text{m}$ ) | 0.425           |
| Weight of SBS between CD28-CD80 and LFA-1-ICAM-1 | $W_{\text{SBS,CC-LI}}$                   | −1.0            |
| Radius of SBS between TCR-pMHC and CD28-CD80     | $R_{\text{SBS,CC-TM}}$ ( $\mu\text{m}$ ) | –               |
| Weight of SBS between TCR-pMHC and CD28-CD80     | $W_{\text{SBS,CC-TM}}$                   | –               |
| Off-rate TCR-pMHC                                | $k_{\text{off,TM}}$ (1/s)                | 0.1             |
| On-rate TCR-pMHC                                 | $k_{\text{on,TM}}$ (1/Ms)                | $2 \times 10^4$ |
| Off-rate LFA-1-ICAM-1                            | $k_{\text{off,LI}}$ (1/s)                | 0.03            |
| On-rate LFA-1-ICAM-1                             | $k_{\text{on,LI}}$ (1/Ms)                | $3 \times 10^5$ |
| Off-rate CD28-CD80                               | $k_{\text{off,CC}}$ (1/s)                | 1.6             |
| On-rate CD28-CD80                                | $k_{\text{on,CC}}$ (1/Ms)                | $4 \times 10^5$ |
| TCR-pMHC centrally directed force                | $C_{\text{TM}}$                          | 1.00            |
| LFA-1-ICAM-1 centrally directed force            | $C_{\text{LI}}$                          | 0.05            |
| CD28-CD80 centrally directed force               | $C_{\text{CC}}$                          | 0.20            |
| Fraction of occupied grid points on the T cell   |                                          | 30%             |
| Fraction of occupied grid points on the SLB      |                                          | 30%             |
| Fraction of TCR, pMHC                            |                                          | 6%              |
| Fraction of CD28, CD80                           |                                          | 9%              |
| Fraction of LFA-1, ICAM-1                        |                                          | 15%             |

line). Actin binding led to a higher concentration of LFA-1-ICAM-1 around the cSMAC that reduced with increasing distance from the center (red dashed line). This quantitatively illustrates the gradient observed in Figure 2Af. The predicted LFA-1 gradient was also found in experiments (Yokosuka et al., 2008). According to the model, actin-mediated forces together with diffusion are responsible for the formation of an LFA-1 gradient in the IS.

The relative positioning of molecules can be quantitatively described using radial distribution functions (RDFs). The RDF between two types represents the frequency of finding a particle of type 2 in a radial neighborhood of type 1 particles. The peak of the RDF of TCR-pMHC complexes to themselves at 60 s reveals the formation of microclusters with a mean diameter ( $d$ ) of  $\approx 3.0 \mu\text{m}$  (Figure 2C). This  $d$  increased and ultimately led to a cSMAC with a  $d$  of  $\approx 2.0$ – $3.0 \mu\text{m}$  at 600 s.

The RDF of LFA1-ICAM-1 complexes around TCR-pMHCs (Figure 2D) also reflects the microclusters with  $d \approx 1 \mu\text{m}$  at 60 s, which evolve to larger structures of  $d \approx 3.0$ – $4.0 \mu\text{m}$  at 600 s. These  $d$ s are larger than those in the RDF of pairs of TCR-pMHC complexes, which reflects the halo around the microclusters and the cSMAC. This predicted halo is also found in experiments, and the model supports that this is a result of membrane bending in these regions (Hartman et al., 2009).

In order to understand the relative effect of actin forces on TCR and LFA-1, the centripetal forces were blocked *in silico* for TCR-

pMHC, but not for LFA-1-ICAM-1. The emerging TCR-pMHC microclusters formed multifocal patterns but failed to merge (Figure S1A). TCR microclusters ended up in a ring structure at the distal SMAC (dSMAC) (Figure S1B). We conclude that for proper IS formation, the centripetal actin-driven force acting on LFA-1 must be lower than that acting on TCR and that the emerging radial LFA-1 gradient affects the localization of other molecules of the IS.

### CD28 Complexes Behave as Passive Followers of TCR-pMHC Movement

Next, we investigated whether LFA-1 would also impact the localization of important signaling molecules such as CD28. The model was extended to include CD28 on the T cell lattice and a CD28 ligand on the APC lattice. In order to compare the *in silico* results with experimental work (Yokosuka et al., 2008), we focused on the ligand CD80. The sizes of the CD28-CD80 and TCR-pMHC complexes are very similar, so we assume no SBS between them and keep the same SBS strength between CD28-CD80 and LFA-1-ICAM-1 as for TCR-pMHC and LFA-1-ICAM-1, unless stated otherwise.

Starting from the configuration in Figure 2Af, CD28-CD80 colocalized with TCR-pMHC complexes in the microclusters. Because of the LFA-1 gradient, most of the CD28-CD80 did not reach the cSMAC. However, a substantial amount passively followed the centripetal movement of TCR-pMHC microclusters



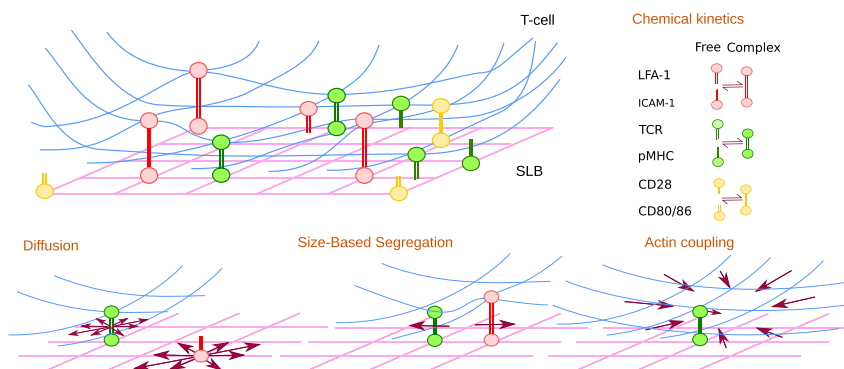


**Figure 1. List of Mechanisms Included in the IS Model**

The membrane of the T cell (blue) and the SLB (pink) carry molecules. Opposite molecules bind or unbind by chemical kinetics. Free and complexed molecules move by diffusion or forces; centripetal forces reflect actin coupling, and SBS represents the effect of membrane bending.

(a behavior not appreciated before), resulting in a small CD28-CD80 ring around the cSMAC (Figures 3Ae–3Ah and 4A, solid line; Video S3). This behavior occurred due to the SBS between CD28-CD80 and LFA-1-ICAM-1 in combination with the TCR-pMHC centripetal flow, which allowed CD28 complexes to follow low tension paths toward the center. The CD28 ring generated by passive following *in silico* was too weak to explain the experimentally observed CD28 ring around the cSMAC (Yokosuka et al., 2008).

### Actin-Dependent Localization of CD28

The effect of a potential actin-driven motion of CD28 complexes (Pielak et al., 2017; Hayashi and Altman, 2006; Tavano et al., 2006) onto its localization was analyzed in the model (Figure 3). SBS between CD28-CD80 and LFA-1-ICAM-1 together with CD28-actin coupling were sufficient to colocalize CD28-CD80 complexes with TCR-pMHC microclusters and to form a CD28 ring around the cSMAC (Figures 3Aa–3Ad, 3B, and 4A, dashed line; Video S4) as in experiment (Yokosuka et al., 2008).

In order to find a criterion that allows to distinguish purely passive following from CD28-CD80 coupling to actin, we investigated how barriers in several shapes that block the diffusion of molecules and complexes on the SLB would influence IS formation (Figure 3C). Colocalization of CD28 and TCR was stronger when CD28 coupling to actin was on. Without actin coupling, most CD28 was located in the dSMAC (Figure 3C). In the annular and square setting, a structural difference was found. With passive following alone, CD28 accumulates on both sides of the barriers (Figure 3C, annular and square), which are low-tension areas due to the accumulation of TCR complexes. Still, a substantial amount of CD28 manages to reach the cSMAC, but less than when actin coupling is on. In this case, CD28 accumulates on the outside of the barriers and in the center of the IS. This is a result of continuous centripetal flow, which is either interrupted by the barrier or guides CD28 into the cSMAC area. Thus, an experiment using such constraints in the SLB would reveal whether CD28 is coupled to actin or not.

CD28 coupling to actin did not change the colocalization of TCR-pMHC and CD28-CD80 early during IS formation (Figure 4A, 60 s). However, after 120 and 300 s, colocalization of CD28 and TCR complexes decreased without actin coupling. With actin coupling, it remained stable and increased after

600 s, when the cSMAC formed. In *in silico* microclusters, CD28 hardly colocalized with TCRs at a distance of less than 210 nm (Figure 4B). This reflects that TCRs move faster to the center than

CD28. However, actin coupling resulted in a higher colocalization of CD28 and TCR in the ring around the cSMAC. To investigate the robustness of these results, additional *in silico* experiments for molecular crowding were performed. The total density of the molecules in Figures 3Aa–3Ad was gradually increased from 30% to 60% (Figure S2A). As expected, this increased the sizes of the cSMAC and CD28 ring (Figure S2A) and consequently pushed the LFA-1 pSMAC further away from the IS center. Despite size changes, the required mechanisms for the formation of the ring-like structure remained the same.

Starting from Figures 3Aa–3Ad, we introduced different densities of an extra population of arbitrary molecules (AMs) without ligands on the SLB on the T cell lattice. Similar to Figure 6, AMs are affected by the LFA-1 gradient in the pSMAC and are excluded to the outer region of the IS. With increasing AM density, CD28 complexes became more spread out around the cSMAC, but the ring-like structure was maintained (Figures S2B and S2D, left graph) based on the same mechanisms of pattern formation.

In order to exclude that the lattice resolution ( $\alpha$ ) of 70 nm would generate artifacts, we replicated the critical simulations with different  $\alpha$ s ( $\alpha = 100, 50$ , and  $35$  nm) (Figure S2C). Additionally, a swapping algorithm was implemented, which allowed agents moving by active forces, such as repulsion and centrally directed force, to exchange positions when two agents are about to move to each other's position (Meyer-Hermann et al., 2012), resulting in a more realistic fluidity similar to a lattice gas model. All the mechanisms and patterns remained in accordance to the reference resolution of  $\alpha = 70$  nm (Figure S3). Altogether, the results show that CD28 coupling to the centripetal actin flow is sufficient for the formation of the ring-like structure and that SBS and passive following alone are not able to generate this pattern.

### Existence of an Optimal Actin Coupling Strength

Next, we asked to which extent actin coupling controls CD28-CD80 localization and varied the coupling strength from complete absence ( $C_{CC} = 0.00$ ), to the strength on TCR complexes ( $C_{CC} = 1.00$ ) (Figure 5). Both TCR and LFA-1 coupling were kept the same as in Figure 2Af. The amount of CD28 in the cSMAC and in the surrounding ring increased with increasing coupling strength (Figure 5B), while the dSMAC population was decreased. The time of pattern formation and the coupling strength were not clearly correlated, and for weak actin coupling,

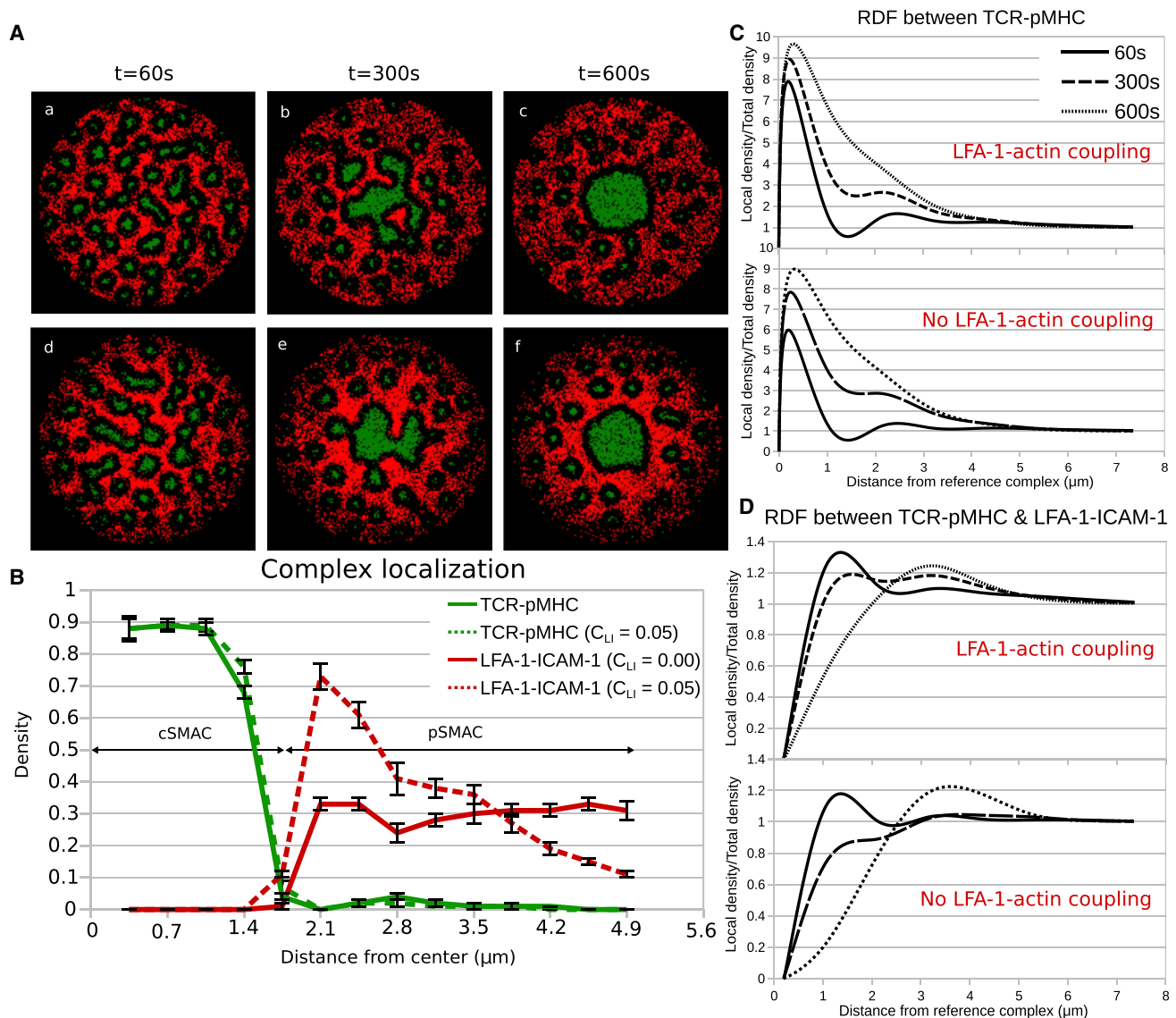


**Figure 2. LFA-1 Coupling to F-actin Induces a Gradient of LFA-1-ICAM-1 Complexes**

(A) IS formation at 60, 300, and 600 s without (a–c) and with (d–f) LFA-1 attachment to F-actin. TCR-pMHC, green; LFA-1-ICAM-1, red.

(B) Radial density profile of complexes along the distance from the center at 600 s, without (solid) or with (dashed) LFA-1 attachment to F-actin. Error bars represent SD.

(C and D) Radial distribution functions at 60, 300, and 600 s between pairs of TCR-pMHC (C) and between TCR-pMHC and LFA-1-ICAM-1 complexes (D) with (top) or without (bottom) LFA-1-actin coupling.

Changed parameters compared to Table 1 are shown. In the absence of CD28 and CD80, the fraction of occupied grid points = 42%, TCR and pMHC = 12%, LFA-1 and ICAM-1 = 30%. In (Aa)–(Ac), ( $C_{LI} = 0.00$ ).

the ring pattern never developed, even at later simulation times. Our analysis suggests that the ring-like structure is a result of the complex combination of (1) SBS between CD28 and LFA-1 complexes, (2) CD28 passively following TCRs, and (3) the centripetal force on CD28 due to actin coupling. We identified an optimal coupling strength of CD28 to actin, which best reproduces the experimentally observed pattern (Yokosuka et al., 2008). Weaker actin coupling ( $C_{CC} = 0.05, 0.10$ ) led to the separation of CD28 into two distinct populations in the cSMAC and the dSMAC (Fig-

ure 5Aa), in contrast to previous findings (Yokosuka et al., 2008). Stronger actin coupling led to an unrealistically high colocalization of CD28 and TCR complexes in the cSMAC and microclusters (Figure 5Af) and the absence of the ring-like pattern of CD28. This shows that the relative localization of CD28-CD80 in the cSMAC versus dSMAC can be tightly regulated by actin forces and that the experimentally observed CD28 ring suggests a substantial actin-driven motion of CD28. Note that the existence of an optimal CD28 coupling strength to actin does not rely on

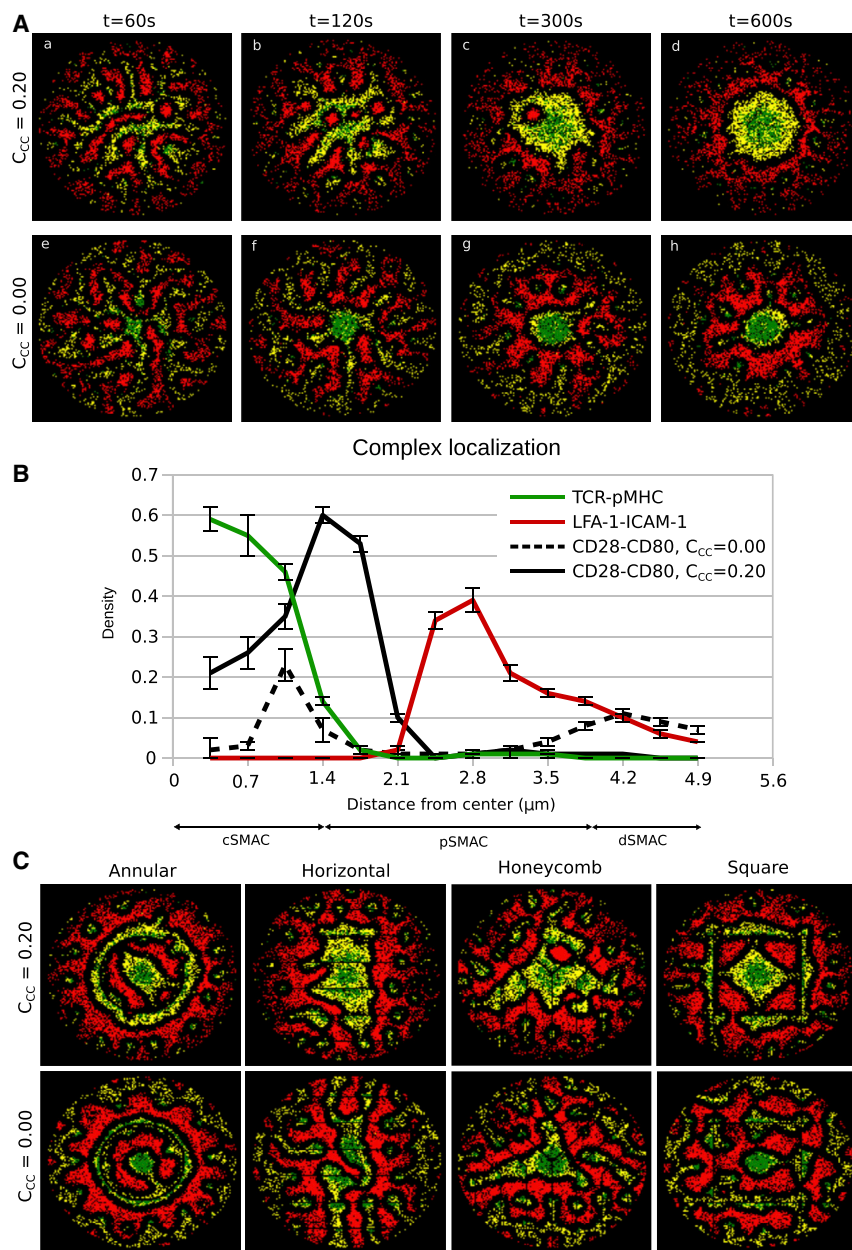


**Figure 3. Effect of CD28-Actin Coupling on the Dynamics of the IS**

(A) IS formation at 60, 120, 300, and 600 s, with (a–d) or without (e–h) CD28-CD80 coupling to actin, in the presence of an LFA-1 gradient.

(B) Radial density profile of complexes along the distance from the center at 600 s, with or without CD28 coupling to actin. Error bars represent SD.

(C) Barriers on the APC lattice that block diffusion of molecules and complexes, with or without CD28 coupling to actin at 600 s. TCR-pMHC, green; LFA-1-ICAM-1, red; CD28-CD80, yellow. Changed parameters compared to Table 1 are shown. In (Ae)–(Ah) and (C, bottom row),  $C_{CC} = 0.00$ .

populations in the cSMAC and dSMAC (Figures 6Ab and 6Ac), in agreement with experimental results. Stronger coupling of LFA-1 to actin excluded more CD28 to the dSMAC, but a substantial amount still remained dispersed throughout the contact region (Figure 6B).

This result applies not only to CD28 but also to any free molecule in the IS (Figure S2B). The modeling results reveal that the predicted LFA-1 gradient, induced by its coupling to the centripetal flow of actin, is a mechanism of dividing free molecules in the IS into two populations relocated to the cSMAC and dSMAC.

## DISCUSSION

We developed a phenomenological agent-based model for investigating the contribution of actin-driven forces to the formation of the synapse and localization of the costimulatory molecule CD28. In the simulations, TCR-pMHC centripetal flow together with the SBS between TCR-pMHC and LFA-1-ICAM-1 led to the formation of microclusters that traveled toward the center, merged into bigger clusters, and finally formed the cSMAC, confirming previous experiments (Grakoui et al., 1999) and

models (Qi et al., 2001; Weikl et al., 2002). Our model predicts that the coupling of LFA-1-ICAM-1 to F-actin induces a gradient of this complex within the pSMAC with a higher density toward the cSMAC. The formation of the gradient relies on the combination of diffusion and actin coupling. The predicted gradient is confirmed in experimental settings (Comrie et al., 2015; Murugesan et al., 2016; Yokosuka et al., 2008). However, its relevance for other molecules in the IS has not been appreciated.

The halo of free space devoid of LFA-1, generated by the SBS between LFA-1 and TCR complexes, allowed TCR to move through the dense pSMAC. Interestingly, complexes with similar size to the TCR were also located in these open areas, allowing them to move through the pSMAC (Figures 3Ae–3Ah). Despite

the LFA-1 gradient in the pSMAC and is also evident in simulations without LFA-1 coupling to actin (Figure S4).

### The LFA-1 Gradient Relocates Free CD28 Molecules

In the absence of CD80, CD28 was observed to spread throughout the IS with a higher accumulation in the dSMAC (Yokosuka et al., 2008). Following this experimental setup, CD80 ligand was removed from the SLB *in silico* such that the free CD28 molecules only diffused on the T cell surface (Figure 6). In the absence of LFA-1 coupling to actin, free CD28 molecules were uniformly spread in the contact region (Figure 6Aa), which is in qualitative disagreement with the experimental result. In contrast, LFA-1 coupling to actin separated free CD28 into two

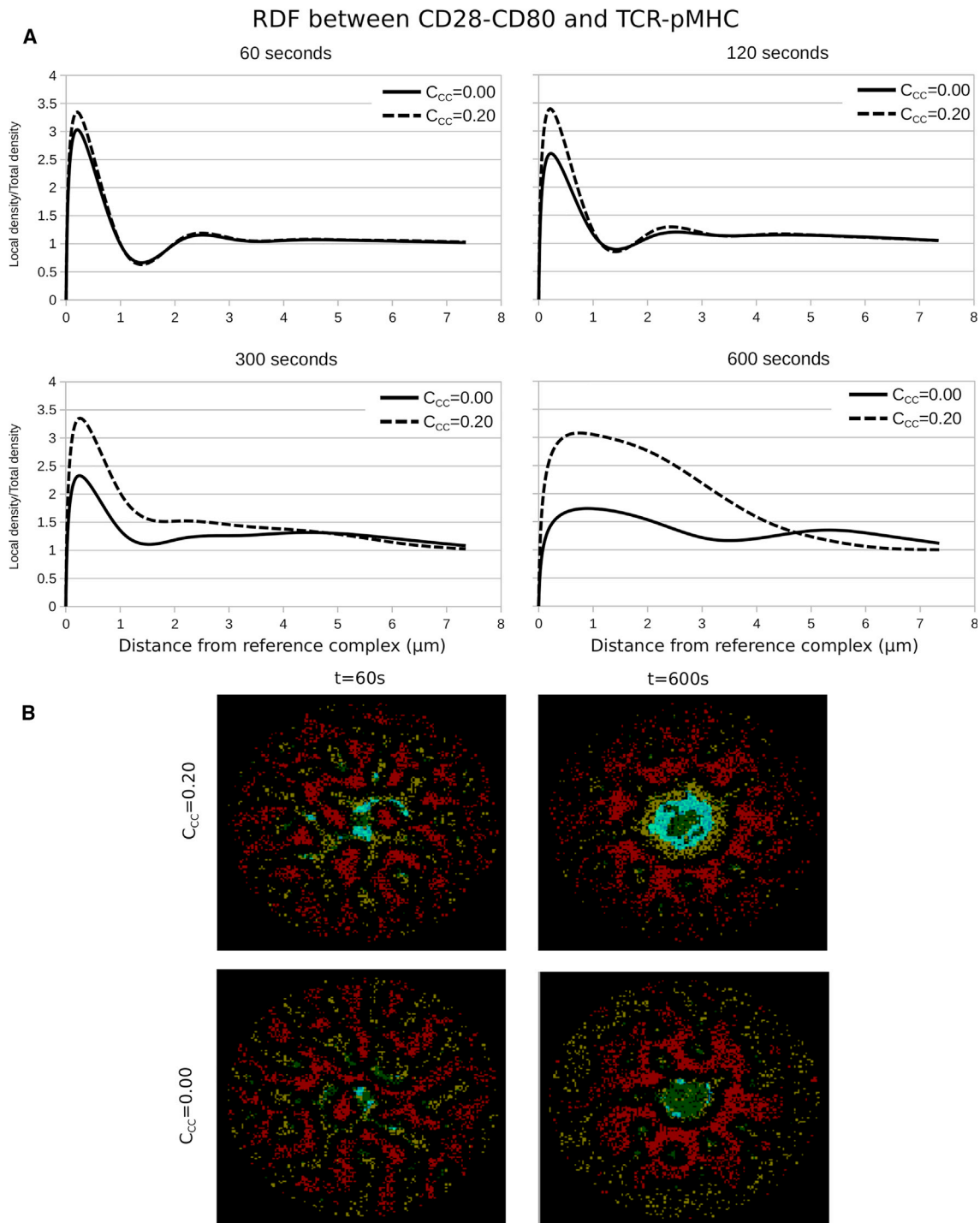


**Figure 4. CD28-Actin Coupling Impacts Colocalization of CD28-CD80 and TCR-pMHC**

(A) Radial distribution function of Figure 3 at 60, 120, 300, and 600 s of IS formation with ( $C_{cc} = 0.20$ ) or without ( $C_{cc} = 0.00$ ) CD28 coupling to actin.

(B) Short-distance colocalization at less than 210 nm (blue) of CD28-CD80 and TCR-pMHC, with ( $C_{cc} = 0.20$ ) or without ( $C_{cc} = 0.00$ ) CD28 coupling to actin. TCR-pMHC, green; LFA-1-ICAM-1, red; CD28-CD80, yellow. Other parameters are as shown in Table 1.

this, the LFA-1 gradient acted as an exclusion mechanism, pushing molecules and complexes away from the pSMAC and toward either the central or distal SMAC (Figures 6 and S2B). This sug-

gests that the LFA-1 gradient impedes molecules escaping or entering the cSMAC. The stronger the coupling of LFA-1 to actin, the more it affected the localization of other molecules (Figures 6).



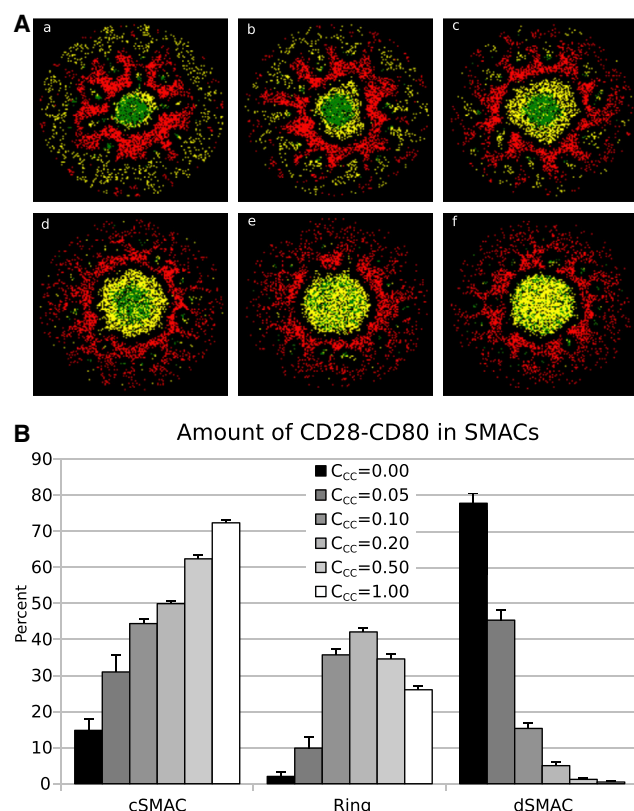


**Figure 5. Variation of the Strength of CD28 Coupling to Actin**  
(A) In (a)–(f), ( $C_{CC} = 0.00, 0.05, 0.10, 0.20, 0.50, 1.00 = C_{TM}$ ), respectively. TCR-pMHC, green; LFA-1-ICAM-1, red; CD28-CD80, yellow.  
(B) Amount of CD28-CD80 complexes in the different regions of the IS, cSMAC, ring around the cSMAC, and dSMAC. Error bars represent SD. Other parameters are as shown in Table 1.

The model predicts that a substantial amount of CD28 complexes behave as passive followers of the TCR-pMHC microcluster movement and localize around the cSMAC (Figures 3Ae–3Ah). This is a result of two mechanisms: SBS of LFA-1-ICAM-1 and CD28-CD80 complexes in the pSMAC, which pushes CD28 complexes into the microclusters, plus actin-driven transport for TCR-pMHC complexes in the microclusters to the cSMAC, which opens low tension paths for CD28 complexes toward the IS center. The model results show that the previously undescribed mechanism of passive following is in parts responsible for the localization of CD28 in a ring around the cSMAC.

Coupling of CD28 to actin was sufficient to guide CD28-CD80 complexes together with the TCR-pMHC microclusters to the cSMAC (Figures 3 and 4) (Yokosuka et al., 2008). The ring-like positioning of CD28 around TCRs was best achieved with an optimal strength of the centripetal flow of CD28-CD80. If coupling of CD28 to actin was too strong, the intermixed pattern in the cSMAC (Figures 5Ae and 5Af) could not be resolved by SBS between CD28-CD80 and TCR-pMHC complexes (see Experimental Procedures) and the ring structure was not restored (Figures S5B and S5C). SBS was unable to affect the

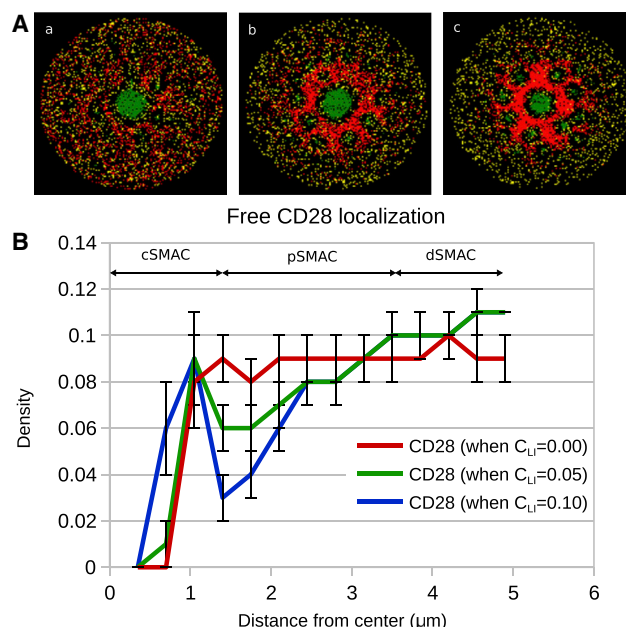


**Figure 6. Impact of the LFA-1 Gradient on Free CD28 Molecules in the Absence of the CD80 Ligand**  
(A) Altering LFA-1 actin coupling strength: (a)  $C_{LI} = 0.00$ , (b)  $C_{LI} = 0.05$ , and (c)  $C_{LI} = 0.10$  at 600 s. TCR-pMHC, green; LFA-1-ICAM-1, red; CD28, yellow.  
(B) Radial density profile of complexes and free CD28 molecules along the distance from the center at 600 s. Error bars represent SD. Other parameters are as shown in Table 1.

ring structure in the IS with optimal CD28 coupling to actin (Figure S5A). Thus, the model predicts that the optimal CD28-CD80 coupling to actin is weaker than for TCR-pMHC. The actin force acts as the regulator of the CD28 distal to central SMAC ratio (Figure 5).

In the *in silico* experiments, TCR-pMHC led the way toward the center of the IS, while CD28-CD80 followed (Figures 3Aa–3Ad and 4B). This suggests an early separation of TCR and CD28 during IS formation. The CD28 ring forms because TCRs reach the center faster. The spatial resolution of the model between 35 and 100 nm allowed for more detailed insight into the nature of surface-molecule movement than current experimental data based on TIRF (total internal reflection fluorescence) microscopy ( $\approx 100$  nm resolution). Therefore, experiments with higher resolution imaging such as STORM (stochastic optical reconstruction microscopy) ( $\approx 20$  nm resolution) would be needed to confirm the early segregation of CD28 and TCR (Rust et al., 2006).

By showing that actin has a critical role in the relative positioning of molecules inside the IS (especially signaling molecules such as TCR, LFA-1, and CD28), our work further suggests that actin helps to bring signaling molecules together and structure signaling pathways in time and space. It has been suggested that TCR signaling is more potent in microclusters than in the cSMAC, which is likely related to the exhaustion of TCR signaling complexes (Beemiller et al., 2012; Hashimoto-Tane et al., 2016, 2017). The model reveals that actin coupling increases the

amount of CD28-CD80 complexes in the vicinity of TCR-pMHC microclusters (Figure 4) and strengthens costimulation in microclusters, as suggested by experimental results (Tavano et al., 2006; Hayashi and Altman, 2006; Yokosuka et al., 2008; Yokosuka and Saito, 2009). In contrast, in the cSMAC, there is colocalization of CD28-CD80 and TCR-pMHC is high when the CD28 ring forms but a low in the inner cSMAC. Together with the presence of phosphorylated PKC $\theta$  around the cSMAC (Yokosuka et al., 2008), this suggests that there is still signaling in that area, but the degree of colocalization deep in the cSMAC decreases and reduces signaling (Varma et al., 2006; Alarcón et al., 2011).

The analysis and implications of transmembrane molecule coupling to actin was in the focus of the presented model. Actin coupling was modeled phenomenologically as a centripetal force acting on molecules (see Experimental Procedures). While this representation is justified for the analysis of IS pattern formation, the mechanisms behind the actin reorientation and transport toward the center of the IS are not considered (Yi et al., 2012). A more explicit representation of the actin dynamics would allow us to go deeper into the coupling mechanisms involved and investigate complex interactions governing binding to actin, such as frictional coupling (DeMond et al., 2008). Our work shows that the strength of coupling to centripetal forces is critical for the organization of the IS, and opens the question whether coupling to actin is a regulated process or could be manipulated by chemical compounds. It would be interesting to assess *in silico* whether this process impacts the speed or coupling of molecules to actin flow.

It should be noted that the physiological interaction between two immune cells involves more complex mechanisms not studied here. The interacting cells build a complex 3D interface with undulating membranes (Cartwright et al., 2014; Oszmiana et al., 2016; Huang et al., 2016; Carisey et al., 2018; Ambler et al., 2017). The cytoskeleton of the APC dynamically changes during IS formation (Benvenuti, 2016), and different APCs can generate ISs with different properties (Nowosad et al., 2016). Actin protrusions in the form of microvilli push parts of the membrane toward the opposite cell, which increases the interaction surface (Cai et al., 2017; Jung et al., 2016). Endo- and exocytosis or recruitment of molecules from the rest of the cell surface to the IS (Martín-Cófreces et al., 2014) further increases the complexity of trafficking dynamics.

This work is designed to reproduce experimental systems relying on SLBs, where molecules on the “virtual APC” side move freely (Figure 1). In this simplified system, actin forces on the T cell side can be studied separately under controlled conditions. High-resolution data of the IS were mostly measured on SLBs, and those imaging data were used to validate the model. For instance, the observed size of microclusters (Hartman et al., 2009; Hashimoto-Tane et al., 2016), the speed of microcluster movement (DeMond et al., 2008), and the speed of cSMAC formation (Grakoui et al., 1999) are consistent with the *in silico* dynamics. Despite the lack of more complex mechanisms, the simplified IS model contains the critical ingredients needed to recapitulate IS formation and is in close agreement with experimental observations based on SLBs (Grakoui et al., 1999; Mossman et al., 2005). As the results of the model were

derived from SLB data, it remains to be proven that the identified mechanisms apply to a 3D T cell-APC IS, which harbors many more complexes with different sizes, such as CTLA-4-CD80/86 and CD2-CD48/58. Further, it has been suggested that F-actin transport occurs within membrane extensions (de la Roche et al., 2016), which would correspond to a space-dependent actin coupling in the model (Köster and Mayor, 2016; Fritzsche et al., 2017).

This work brings new insights into the mechanistic foundations of a mature IS. It can reproduce the localization of a variety of complexes interacting with their surroundings in T cells on SLBs. We showed that the mechanism of actin coupling can not only generate complex patterns, such as the LFA-1 pSMAC gradient or the CD28 ring structure, but also segregate complexes with different coupling strengths, such as TCR-pMHC and CD28-CD80, despite their similar size. The presented model is a suitable tool to further investigate signaling events on the T cell. It can help us to not only better understand the effect that targeted molecules can have on T cell signaling based on their localization in the IS but also predict new mechanisms that are not currently discussed or not yet considered important for the formation of such characteristic patterns. The localization of CD28-CD80 around the cSMAC could be used to study its effect on calcium flux as well as phosphorylation of PKC $\theta$  and how this leads to T cell activation.

## EXPERIMENTAL PROCEDURES

The *in silico* simulations were made to replicate the experimental procedures of the IS study (Grakoui et al., 1999), where T cells are activated on top of SLBs containing floating pMHC and ICAM-1 (also CD80, etc.) as a simplified representation of an APC surface. The *in silico* procedure begins by representing the interaction surface of the two membranes of the experiment, the T cell plasma membrane and the SLB (Figure 1). For the sake of simplicity, and since the impact of membrane deformation is not explicitly modeled, both surfaces are described in two dimensions (2D). Therefore, two lattices are created as square meshes. The nodes of the lattices (grid points) are initially empty. Each grid point has eight neighbors (Moore neighborhood), and the agents will roam on these grid points.

The agents are the molecules under consideration, which are uniformly distributed on the two lattices. Each grid point can be occupied by a maximum of one agent. The agents randomly move between neighboring grid-point positions according to their diffusion coefficient. Diffusion is implemented as a random walk with a probability defined by the speed of diffusion and the simulation time step. Because diagonal movements are longer than horizontal or vertical ones, the probability of diagonal movements is reduced by the factor  $\sqrt{1/2}$ .

Free molecules can find a ligand on the other lattice and form a complex. Only ligands on the exact same position are considered. The binding probability is defined by the specific binding rates and the volume of the complex that is about to form (Figure S1C). Complexes can unbind and return to the free-molecule state with a probability defined by the dissociation rates of each specific complex. When a complex diffuses, its two agents (one on each lattice) need to move in the same direction, which happens less frequently. The diffusion rate of the complexes is thus assumed lower than that of free molecules,  $D_c < D_m$ , where c denotes complex and m molecule. In order to avoid artificial inhibition of motility by local crowdedness, a local exchange algorithm was implemented (Meyer-Hermann et al., 2012); agents that failed to move by active forces (SBS or actin coupling) to an occupied node are stored on a list. At the end of each time step, each agent on this list checks its target position again and moves if it is free. If the target position is occupied by an agent with a force pointing toward the moving agent, then the agents are exchanged. Otherwise, the agent remains in its position. SBS assumes that the size difference of complexes induces membrane deformations. This is translated into a repulsive force

between long (LFA-1-ICAM-1) and short (TCR-pMHC or CD28-CD80) complexes. This force is modeled as a weighted vector from a complex toward all its interacting neighbors, within a radius  $R_{\text{force}}$ . The weight of each vector represents the strength of the force relative to diffusion. Negative weights represent repulsion, and positive ones represent attraction. The weights for TCR-pMHC and LFA-1-ICAM-1 interactions were taken from Figge and Meyer-Hermann (2009) (Table 1). All vectors are summed, and the resulting vector points to the direction of movement. The direction is attributed to one of the eight neighbors, based on a probabilistic function (Siokis et al., 2017).

Since the model is in 2D, a way to represent the transport of complexes by the centripetal contraction of the F-actin arcs is needed. The transport of complexes by the centripetal contraction of F-actin arcs is modeled as a centrally directed empirical force. It is added to the SBS force vector with weight  $C_x > 0$ , where  $X$  denotes the specific complex, which reflects the strength of the F-actin binding. The amount of CD80 was varied between 60% and 120% of the amount of ICAM-1 (Table 1; Yokosuka et al., 2008). As the results remained similar (Figure S6), a value of 60% was used. The size of the CD28-CD80 complex is very close to that of TCR-pMHC,  $L_{CC} \approx 15\text{nm}$ . Therefore, SBS between CD28-CD80 and LFA-1-ICAM-1 complexes was assumed. The dissociation constant for CD28-CD80 complexes is  $k_d = 4\ \mu\text{M}$ , with  $k_{\text{off}} \geq 1.6\text{s}^{-1}$  and  $k_{\text{on}} \geq 4 \times 10^5\text{M}^{-1}\text{s}^{-1}$  (Figure S7; van der Merwe et al., 1997). All of the parameters used in the presented simulations are shown in Table 1. For a more systematic explanation of the simulation procedure, the reader may refer to Siokis et al. (2017).

The RDF (or pair correlation function) describes the density as a function of distance from a reference particle. In this study, we implemented the RDF as the local density of particles (complexes or molecules) inside a ring of width  $dr$ , at a distance  $r$  from a reference particle, normalized by the total density of the particle under consideration. The plotted RDF represents the frequency of finding a particle of a specific type in a particular distance from a reference particle. This representation is useful to show the mean size of TCR-pMHC microclusters (Figure 2C), the distribution of LFA-1-ICAM-1 away from a TCR-pMHC microcluster (Figure 2D), and the degree of colocalization of CD28-CD80 and TCR-pMHC in microclusters (Figure 4A). The model further allows calculation of the amount of molecules or complexes within a defined radius  $R_{\text{col}} = 0.21\ \mu\text{m}$ . If a minimum number  $\min(X, Y) \geq 7 * (\alpha_0 / \alpha)$ , where  $\alpha_0 = 70\text{nm}$  is the reference lattice resolution and  $\alpha$  is the resolution of the current simulation, of the two different kinds of molecules or complexes  $X$  and  $Y$  is found within this radius, then these molecules are counted as colocalized (Figure 4B). The presented agent-based simulations could also be implemented as a PDE model by treating the IS on a macroscopic population level. We chose an agent-based model, because this allows us to represent the single-molecule level, which might become relevant in small structures and at high resolution. In this limit, agent-based approaches appear as the better choice. Effects like passive following appear as a natural result of the agent-based model, which is less easily obtained by a PDE approach.

## DATA AND SOFTWARE AVAILABILITY

The code is written in C++ according to all the algorithmic details explained in Siokis et al. (2017) and is available upon request.

## SUPPLEMENTAL INFORMATION

Supplemental Information includes seven figures and four videos and can be found with this article online at <https://doi.org/10.1016/j.celrep.2018.06.114>.

## ACKNOWLEDGMENTS

This work was supported by the Human Frontier Science Program (RGP0033/2015), the Kennedy Trust for Rheumatology Research (P.D.), and the Wellcome Trust Fellowship (100262Z/12/Z) (M.L.D.).

## AUTHOR CONTRIBUTIONS

A.S., P.A.R., P.D., M.L.D., and M.M.-H. conceived and designed the study. A.S. designed the code and performed and analyzed the simulations. P.A.R.

and M.M.-H. supervised the work. A.S., P.A.R., P.D., M.L.D., and M.M.-H. wrote and edited the manuscript.

## DECLARATION OF INTERESTS

The authors declare no competing interests.

Received: January 1, 2018

Revised: April 18, 2018

Accepted: June 28, 2018

Published: July 31, 2018

## REFERENCES

- Acuto, O., and Michel, F. (2003). CD28-mediated co-stimulation: a quantitative support for TCR signalling. *Nat. Rev. Immunol.* 3, 939–951.
- Alarcón, B., Mestre, D., and Martínez-Martín, N. (2011). The immunological synapse: a cause or consequence of T-cell receptor triggering? *Immunology* 133, 420–425.
- Ambler, R., Ruan, X., Murphy, R.F., and Wülfing, C. (2017). Systems imaging of the immune synapse. In *The Immune Synapse: Methods and Protocols*, C.T. Baldari and M.L. Dustin, eds. (Springer), pp. 409–421.
- Babich, A., Li, S., O'Connor, R.S., Milone, M.C., Freedman, B.D., and Burkhardt, J.K. (2012). F-actin polymerization and retrograde flow drive sustained PLC $\gamma$ 1 signaling during T cell activation. *J. Cell Biol.* 197, 775–787.
- Basu, R., and Huse, M. (2017). Mechanical communication at the immunological synapse. *Trends Cell Biol.* 27, 241–254.
- Beemiller, P., Jacobelli, J., and Krummel, M.F. (2012). Integration of the movement of signaling microclusters with cellular motility in immunological synapses. *Nat. Immunol.* 13, 787–795.
- Benvenuti, F. (2016). The dendritic cell synapse: a life dedicated to t cell activation. *Front. Immunol.* 7, 70.
- Beyersdorf, N., Kerkau, T., and Hünig, T. (2015). CD28 co-stimulation in T-cell homeostasis: a recent perspective. *ImmunoTargets Ther.* 4, 111–122.
- Bromley, S.K., Iaboni, A., Davis, S.J., Whitty, A., Green, J.M., Shaw, A.S., Weiss, A., and Dustin, M.L. (2001). The immunological synapse and CD28-CD80 interactions. *Nat. Immunol.* 2, 1159–1166.
- Burroughs, N.J., and Wülfing, C. (2002). Differential segregation in a cell-cell contact interface: the dynamics of the immunological synapse. *Biophys. J.* 83, 1784–1796.
- Cai, E., Marchuk, K., Beemiller, P., Beppler, C., Rubashkin, M.G., Weaver, V.M., Gérard, A., Liu, T.-L., Chen, B.-C., Betzig, E., et al. (2017). Visualizing dynamic microvillar search and stabilization during ligand detection by T cells. *Science* 356, eaal3118.
- Carisey, A.F., Mace, E.M., Saeed, M.B., Davis, D.M., and Orange, J.S. (2018). Nanoscale dynamism of actin enables secretory function in cytolytic cells. *Curr. Biol.* 28, 489–502.e9.
- Carlson, A., and Mahadevan, L. (2015). Elastohydrodynamics and kinetics of protein patterning in the immunological synapse. *PLoS Comput. Biol.* 11, e1004481.
- Cartwright, A.N., Griggs, J., and Davis, D.M. (2014). The immune synapse clears and excludes molecules above a size threshold. *Nat. Commun.* 5, 5479.
- Comrie, W.A., Babich, A., and Burkhardt, J.K. (2015). F-actin flow drives affinity maturation and spatial organization of LFA-1 at the immunological synapse. *J. Cell Biol.* 208, 475–491.
- de la Roche, M., Asano, Y., and Griffiths, G.M. (2016). Origins of the cytolytic synapse. *Nat. Rev. Immunol.* 16, 421–432.
- DeMond, A.L., Mossman, K.D., Starr, T., Dustin, M.L., and Groves, J.T. (2008). T cell receptor microcluster transport through molecular mazes reveals mechanism of translocation. *Biophys. J.* 94, 3286–3292.
- Dustin, M.L. (2014). What counts in the immunological synapse? *Mol. Cell* 54, 255–262.
- Dustin, M.L., and Depoil, D. (2011). New insights into the T cell synapse from single molecule techniques. *Nat. Rev. Immunol.* 11, 672–684.



- Figge, M.T., and Meyer-Hermann, M. (2006). Geometrically repatterned immunological synapses uncover formation mechanisms. *PLoS Comput. Biol.* 2, e171.
- Figge, M., and Meyer-Hermann, M. (2009). Modeling receptor-ligand binding kinetics in immunological synapse formation. *Eur. Phys. J. D* 51, 153–160.
- Fritzsche, M., Fernandes, R.A., Chang, V.T., Colin-York, H., Clausen, M.P., Felce, J.H., Galiani, S., Erlenkämper, C., Santos, A.M., Heddleston, J.M., et al. (2017). Cytoskeletal actin dynamics shape a ramifying actin network underpinning immunological synapse formation. *Sci. Adv.* 3, e1603032.
- Grakoui, A., Bromley, S.K., Sumen, C., Davis, M.M., Shaw, A.S., Allen, P.M., and Dustin, M.L. (1999). The immunological synapse: a molecular machine controlling T cell activation. *Science* 285, 221–227.
- Hartman, N.C., Nye, J.A., and Groves, J.T. (2009). Cluster size regulates protein sorting in the immunological synapse. *Proc. Natl. Acad. Sci. USA* 106, 12729–12734.
- Hashimoto-Tane, A., Sakuma, M., Ike, H., Yokosuka, T., Kimura, Y., Ohara, O., and Saito, T. (2016). Micro-adhesion rings surrounding TCR microclusters are essential for T cell activation. *J. Exp. Med.* 213, 1609–1625.
- Hashimoto-Tane, A., Yokosuka, T., and Saito, T. (2017). Analyzing the dynamics of signaling microclusters. In *The Immune Synapse: Methods and Protocols*, C.T. Baldari and M.L. Dustin, eds. (Springer), pp. 51–64.
- Hayashi, K., and Altman, A. (2006). Filamin A is required for T cell activation mediated by protein kinase C- $\theta$ . *J. Immunol.* 177, 1721–1728.
- Hori, Y., Raychaudhuri, S., and Chakraborty, A.K. (2002). Analysis of pattern formation and phase separation in the immunological synapse. *J. Chem. Phys.* 117, 9491–9501.
- Huang, J., Zeng, X., Sigal, N., Lund, P.J., Su, L.F., Huang, H., Chien, Y.H., and Davis, M.M. (2016). Detection, phenotyping, and quantification of antigen-specific T cells using a peptide-MHC dodecamer. *Proc. Natl. Acad. Sci. USA* 113, E1890–E1897.
- Jung, Y., Riven, I., Feigelson, S.W., Kartvelishvili, E., Tohya, K., Miyasaka, M., Alon, R., and Haran, G. (2016). Three-dimensional localization of T-cell receptors in relation to microvilli using a combination of superresolution microscopies. *Proc. Natl. Acad. Sci. USA* 113, E5916–E5924.
- Köster, D.V., and Mayor, S. (2016). Cortical actin and the plasma membrane: inextricably intertwined. *Curr. Opin. Cell Biol.* 38, 81–89.
- Lee, K.-H., Holdorf, A.D., Dustin, M.L., Chan, A.C., Allen, P.M., and Shaw, A.S. (2002). T cell receptor signaling precedes immunological synapse formation. *Science* 295, 1539–1542.
- Lee, K.-H., Dinner, A.R., Tu, C., Campi, G., Raychaudhuri, S., Varma, R., Sims, T.N., Burack, W.R., Wu, H., Wang, J., et al. (2003). The immunological synapse balances T cell receptor signaling and degradation. *Science* 302, 1218–1222.
- Manz, B.N., Jackson, B.L., Petit, R.S., Dustin, M.L., and Groves, J. (2011). T-cell triggering thresholds are modulated by the number of antigen within individual T-cell receptor clusters. *Proc. Natl. Acad. Sci. USA* 108, 9089–9094.
- Martín-Cófreces, N.B., Baixaui, F., and Sánchez-Madrid, F. (2014). Immune synapse: conductor of orchestrated organelle movement. *Trends Cell Biol.* 24, 61–72.
- Meyer-Hermann, M., Mohr, E., Pelletier, N., Zhang, Y., Vitorica, G.D., and Toellner, K.-M. (2012). A theory of germinal center B cell selection, division, and exit. *Cell Rep.* 2, 162–174.
- Mossman, K.D., Campi, G., Groves, J.T., and Dustin, M.L. (2005). Altered TCR signaling from geometrically repatterned immunological synapses. *Science* 310, 1191–1193.
- Murugesan, S., Hong, J., Yi, J., Li, D., Beach, J.R., Shao, L., Meinhardt, J., Madison, G., Wu, X., Betzig, E., and Hammer, J.A. (2016). Formin-generated actomyosin arcs propel T cell receptor microcluster movement at the immune synapse. *J. Cell Biol.* 215, 383–399.
- Nowosad, C.R., Spillane, K.M., and Tolar, P. (2016). Germinal center B cells recognize antigen through a specialized immune synapse architecture. *Nat. Immunol.* 17, 870–877.
- Ortega-Carrion, A., and Vicente-Manzanares, M. (2016). Concerning immune synapses: a spatiotemporal timeline. *F1000Res.* 5, F1000 Faculty Rev-418.
- Oszmiana, A., Williamson, D.J., Cordoba, S.-P., Morgan, D.J., Kennedy, P.R., Stacey, K., and Davis, D.M. (2016). The size of activating and inhibitory killer Ig-like receptor nanoclusters is controlled by the transmembrane sequence and affects signaling. *Cell Rep.* 15, 1957–1972.
- Pentcheva-Hoang, T., Egen, J.G., Wojnoonski, K., and Allison, J.P. (2004). B7-1 and B7-2 selectively recruit CTLA-4 and CD28 to the immunological synapse. *Immunity* 21, 401–413.
- Pielak, R.M., O'Donoghue, G.P., Lin, J.J., Alfieri, K.N., Fay, N.C., Low-Nam, S.T., and Groves, J.T. (2017). Early T cell receptor signals globally modulate ligand:receptor affinities during antigen discrimination. *Proc. Natl. Acad. Sci. USA* 114, 12190–12195.
- Qi, S.Y., Groves, J.T., and Chakraborty, A.K. (2001). Synaptic pattern formation during cellular recognition. *Proc. Natl. Acad. Sci. USA* 98, 6548–6553.
- Rust, M.J., Bates, M., and Zhuang, X. (2006). Sub-diffraction-limit imaging by stochastic optical reconstruction microscopy (STORM). *Nat. Methods* 3, 793–795.
- Sage, P.T., Varghese, L.M., Martinelli, R., Sciuto, T.E., Kamei, M., Dvorak, A.M., Springer, T.A., Sharpe, A.H., and Carman, C.V. (2012). Antigen recognition is facilitated by invadosome-like protrusions formed by memory/effector T cells. *J. Immunol.* 188, 3686–3699.
- Sanchez-Lockhart, M., Graf, B., and Miller, J. (2008). Signals and sequences that control CD28 localization to the central region of the immunological synapse. *J. Immunol.* 181, 7639–7648.
- Sansom, D.M., and Walker, L.S. (2006). The role of CD28 and cytotoxic T-lymphocyte antigen-4 (CTLA-4) in regulatory T-cell biology. *Immunol. Rev.* 212, 131–148.
- Siokis, A., Robert, P.A., and Meyer-Hermann, M. (2017). Mathematical modeling of synaptic patterns. In *The Immune Synapse: Methods and Protocols*, C.T. Baldari and M.L. Dustin, eds. (Springer), pp. 171–182.
- Slavik, J.M., Hutchcroft, J.E., and Bierer, B.E. (1999). CD80 and CD86 are not equivalent in their ability to induce the tyrosine phosphorylation of CD28. *J. Biol. Chem.* 274, 3116–3124.
- Springer, T.A. (1990). Adhesion receptors of the immune system. *Nature* 346, 425–434.
- Tabdanov, E., Gondarenko, S., Kumari, S., Liapis, A., Dustin, M.L., Sheetz, M.P., Kam, L.C., and Iskratsch, T. (2015). Micropatterning of TCR and LFA-1 ligands reveals complementary effects on cytoskeleton mechanics in T cells. *Integr. Biol.* 7, 1272–1284.
- Tavano, R., Contento, R.L., Baranda, S.J., Soligo, M., Tuosto, L., Manes, S., and Viola, A. (2006). CD28 interaction with filamin-A controls lipid raft accumulation at the T-cell immunological synapse. *Nat. Cell Biol.* 8, 1270–1276.
- Tseng, S.-Y., Liu, M., and Dustin, M.L. (2005). CD80 cytoplasmic domain controls localization of CD28, CTLA-4, and protein kinase C $\theta$  in the immunological synapse. *J. Immunol.* 175, 7829–7836.
- Tseng, S.-Y., Waite, J.C., Liu, M., Vardhana, S., and Dustin, M.L. (2008). T cell-dendritic cell immunological synapses contain TCR-dependent CD28-CD80 clusters that recruit protein kinase C  $\theta$ . *J. Immunol.* 181, 4852–4863.
- Tsourkas, P.K., and Raychaudhuri, S. (2010). Modeling of B cell synapse formation by Monte Carlo simulation shows that directed transport of receptor molecules is a potential formation mechanism. *Cell. Mol. Bioeng.* 3, 256–268.
- Tsourkas, P.K., Baumgarth, N., Simon, S.I., and Raychaudhuri, S. (2007). Mechanisms of B-cell synapse formation predicted by Monte Carlo simulation. *Biophys. J.* 92, 4196–4208.
- van der Merwe, P.A., Bodian, D.L., Daenke, S., Linsley, P., and Davis, S.J. (1997). CD80 (B7-1) binds both CD28 and CTLA-4 with a low affinity and very fast kinetics. *J. Exp. Med.* 185, 393–403.
- Varma, R., Campi, G., Yokosuka, T., Saito, T., and Dustin, M.L. (2006). T cell receptor-proximal signals are sustained in peripheral microclusters and terminated in the central supramolecular activation cluster. *Immunity* 25, 117–127.
- Wang, C.J., Heuts, F., Ovcinnikovs, V., Wardzinski, L., Bowers, C., Schmidt, E.M., Kogimtzis, A., Kenefack, R., Sansom, D.M., and Walker, L.S. (2015).



- CTLA-4 controls follicular helper T-cell differentiation by regulating the strength of CD28 engagement. *Proc. Natl. Acad. Sci. USA* 112, 524–529.
- Weikl, T., Groves, J., and Lipowsky, R. (2002). Pattern formation during adhesion of multicomponent membranes, *EPL. Europhys. Lett.* 59, 916.
- Yi, J., Wu, X.S., Crites, T., and Hammer, J.A., 3rd. (2012). Actin retrograde flow and actomyosin II arc contraction drive receptor cluster dynamics at the immunological synapse in Jurkat T cells. *Mol. Biol. Cell* 23, 834–852.
- Yokosuka, T., and Saito, T. (2009). Dynamic regulation of T-cell costimulation through TCR-CD28 microclusters. *Immunol. Rev.* 229, 27–40.
- Yokosuka, T., Kobayashi, W., Sakata-Sogawa, K., Takamatsu, M., Hashimoto-Tane, A., Dustin, M.L., Tokunaga, M., and Saito, T. (2008). Spatiotemporal regulation of T cell costimulation by TCR-CD28 microclusters and protein kinase C  $\theta$  translocation. *Immunity* 29, 589–601.
- Yu, Y., Smoligovets, A.A., and Groves, J.T. (2013). Modulation of T cell signaling by the actin cytoskeleton. *J. Cell Sci.* 126, 1049–1058.